Preprint Title Structural and optical characteristics designed by sputtering deposition conditions of the oxide thin films

Authors Petronela Prepelita, Florin Garoi and Valentin Craciun

Publication Date 02 Nov 2020

Article Type Full Research Paper

ORCID® iDs Petronela Prepelita - https://orcid.org/0000-0002-9636-1091; Florin Garoi - https://orcid.org/0000-0003-0448-6688

Structural and optical characteristics designed by sputtering deposition conditions of the oxide thin films

Petronela Prepelita*[1], Florin Garoi[1], and Valentin Craciun[1]

Address: [1]National Institute for Laser, Plasma and Radiation Physics, 409 Atomistilor Street, PO Box MG-36, Magurele 077125, Ilfov, Romania

Email: Petronela Prepelita (married as Garoi) - petronela.garoi@inflpr.ro

* Corresponding author

Abstract

The influence of film thickness on the structural and optical properties of silicon dioxide (SiO_2) and zinc oxides (ZnO) thin films deposited by radio frequency magnetron sputtering on quartz substrates was investigated. Deposition conditions were optimized to achieve stoichiometric thin films. The orientation of crystallites, structure and composition were investigated by X-ray diffraction (XRD) and X-ray photoelectron spectroscopy (XPS), while the surface topography of samples was analyzed using scanning electron microscopy (SEM). The optical characteristics were measured for samples with the same composition but obtained with different deposition parameters, such as increasing thickness. Optical constants (i.e. refractive index *n*, extinction coefficient *k*, and absorption coefficient *α*) of the SiO_2 and ZnO oxide films were determined using Swanepoel's method from the transmission spectra recorded in the

range 190 - 2500 nm, while the energy bandgap was calculated from the absorption spectra. The influence of thickness on the structural and optical properties of the oxide films was investigated. A good optical quality and real performance was noticed, which makes these thin films deem worthy of integration into metamaterial structures.

Keywords

SiO_2 and ZnO, thin films, magnetron sputtering, structural properties, optical quality

Introduction

The research into oxide thin films is quite diverse due to their excellent properties [1-5], such as dielectric properties [6-8] for the production of metamaterials [9]. Metamaterials applied in the field of space science come with a new dimension of microstructural representation of the advanced functional materials [10,11]. Materials with dielectric qualities, such as SiO_2 and ZnO, are used to make devices with metasurface structures in the broad visible spectral domain. They are intensely investigated due to their versatile properties, such as: high transmissions in the visible range [12,13], energy bandgap [14-16], etc. Among the important applications of these oxides are: materials with dielectric properties into the metasurface structures; transparent conductive oxides and buffer layers in solar cells technology; materials into the sensor technology, etc. [6,8,17-21]. As materials with dielectric properties, SiO_2 and ZnO, exhibit a dependence of the electrical resistance with temperature [22,23].

The SiO_2 and ZnO films are obtained by various deposition techniques, such as: matrix-assisted pulsed laser evaporation (MAPLE) [24,25], spin coating of sol-gel precursor solutions [26], radio frequency magnetron sputtering (rfMS) [27-30], vacuum thermal evaporation (VTE) [31-33], chemical methods [34], reactive ion beam sputter

deposition [35] etc. For example, SiO_2 and ZnO films obtained by rfMS technique can be used as dielectric materials in metasurface structures, or as dielectric interfaces into the structure of a metamaterial.

This paper reports the experimental conditions for deposition of ZnO and SiO_2 films, as an improvement of rfMS vacuum deposition technique for dielectric layers (e.g. ZnO and SiO_2) onto quartz substrates. Here we investigated SiO_2 and ZnO thin films with thicknesses ranging from 200 nm to 300 nm. Thus, we analyzed the beneficial effect of increasing the film thickness on the composition, morphology, structure and spectral characteristics of the studied samples. This way of analyzing oxide thin film thickness dependence on the optical and structural characteristics, allows us to clearly point out their necessity in metamaterial structures.

Experimental

The VARIAN ER 3119 EletroRava (INFLPR) deposition installation is provided with a deposition chamber, two magnetrons and *in situ* thickness monitoring. Thus, radio frequency magnetron sputtering (rfMS) technique [27,36,37] was used to deposit the SiO_2 and ZnO oxide films. This ensures deposition on large areas and quality thin films for multiple applications. They are achieved at room temperature on quartz substrates with thickness ranging from 200 nm to 300 nm, from targets in the form of a disk with 4″ diameter and 0.125″ thickness (SiO_2 and ZnO individually sintered, 99.99% purity from Lesker). Working gases (i.e. argon, 95% and oxygen, 5%) were introduced in the deposition chamber via a circuit provided with flow meters (30 sccm and 1.5 sccm, respectively), in order to precisely control and regulate the flow of gases into the deposition chamber. Quartz (fused silica, NEGS2) slides with dimensions of 2 cm × 2 cm × 0.1 cm were used as substrates. Initially, all substrates were cleaned in an

ultrasonic bath to ensure good reproducibility of the properties of thin films. Subsequently, the substrates were kept in special mounts on the rotating metallic plate, above the deposition targets. The rfMS method results in uniform growth of the oxide films and a good control of their composition.

To characterize the structure and thickness of the deposited SiO_2 and ZnO thin films several methods were applied, including X-ray photoelectron spectroscopy (XPS), X-ray diffraction (XRD), and scanning electron microscopy (SEM). Hence, the ESCALAB 250+ XPS equipment was used to determine the surface composition of the samples, with the following specifications: monochromatic radiation Al Kα (1486.6 eV) and vacuum in the analysis chamber, p ~ 1.6×10^{-10} mbar. The XRD analysis was performed using a Brucker D8 Advance diffractometer. The crystalline structure of oxide thin films was investigated by the standard XRD technique, using Cu Kα radiation (λ = 1.55418 Å) in the range of 2θ = 25 – 80 degrees.

Using SEM technique, we studied the surface of the samples at different magnifications, by scanning them with a beam of accelerated electrons to very high energies (~ 20 keV). The structural quality and surfaces morphology were investigated using a scanning electron microscope (FEI Co., model Inspect S50). The system is equipped with X-ray source and EDX unit with elementary energy dispersion spectroscopy (EDS). These analyzes employ different magnifications depending on the quality of the thin films and structure of their surface. Using the cross-section imaging and a magnification of 20 000 ×, it was possible to gain information related to the thickness of our samples.

Optical transmission spectra were acquired using a UV-VIS-NIR Perkin-Elmer Lambda 950 Spectrophotometer, with a measuring range between 190 nm and 2500 nm, and a wavelength accuracy of 0.08 nm in UV-VIS and 0.3 nm in NIR band respectively.

Results

X-ray diffraction analysis of oxide samples was realized in the range of angles 25 – 80 degrees (Fig.1). It was performed to determine the type of structure (e.g. polycrystalline or amorphous) and orientation of the thin films. Figure 1 shows typical XRD patterns of ZnO thin films with increasing thickness and prepared by rfMS process. Following the effect of deposition parameters of the oxide films we found that diffractograms show increasing intensities of the peaks with thickness, determining an improvement of their crystalline structure. In the case of ZnO samples, the crystalline phases and peaks were identified as corresponding to (002) and (004) planes, according to JCPDS XRD the standard diffractograms [38]. These diffractograms indicate good crystalline quality and the analyzed films show two diffraction peaks, characteristic of the ZnO hexagonal structure (wurtzite). The studied thin films have a crystalline structure with a strong orientation of the planes (002) parallel to the surface of the substrates.

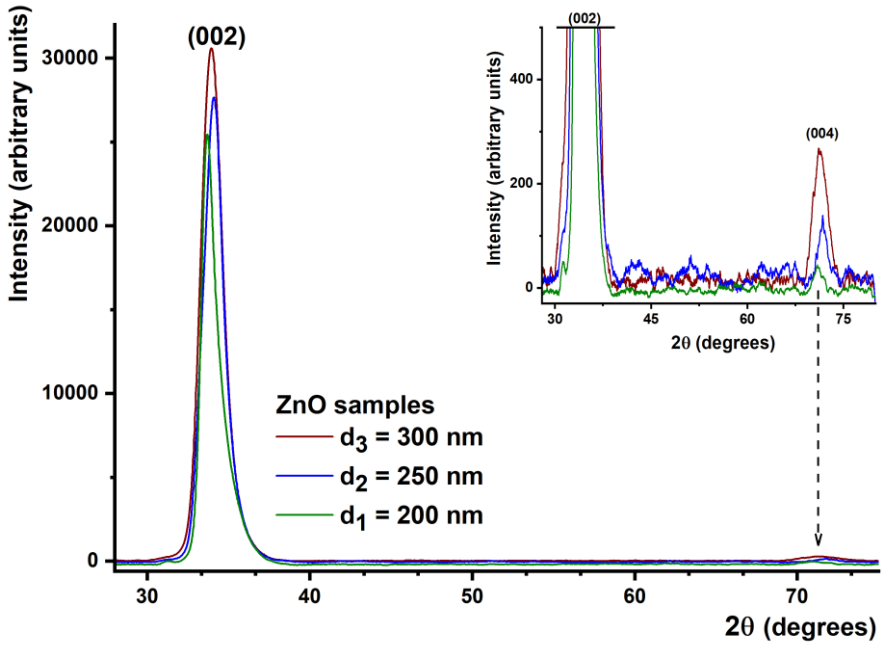

Fig. 1 XRD patterns of the ZnO thin film samples with different thickness, namely: 200 nm, 250 nm and 300nm.

In the diffractogram of the 200 nm thick film, diffraction peaks corresponding to a single-phase growth of the film were initially identified. Low intensities of the diffraction lines (004) are due to growth stress, which is unevenly distributed in the film. In the diffractogram corresponding to the 250 nm thick film it can be seen how the film grew oriented with the c-axis perpendicular to the substrate surface, a phenomenon that is specific to depositions made at room temperature.

The values of the (002) plane, corresponding to the multiple reflections on the substrate surface, for ZnO thin films are presented in Table 1. One of the films of the highest quality in terms of structure was the one deposited at a thickness of 300 nm; this is consistent with the value of the lattice parameter c = 5.2090 Å, indicating a good oxygenation.

Table 1. XRD results for ZnO thin films with different thickness values.

sample	***d*** **(nm)**	**(hkl)**	***2θ*** **(°)**	***β*$_{2\theta}$** **(mrad)**	***D*** **(nm)**	***d*$_{hkl}$** **(Å)**	***c*** **(Å)**	***ε2*** **(%)**	**TC (hkl)**
ZnO200	200	(002)	34.42	20.2	7.19	2.604	5.209	0.088	1.82
		(004)	72.57	26.9	6.39	1.302	5.208	0.069	1.05
ZnO250	250	(002)	34.43	26.2	5.53	2.604	5.208	0.067	1.98
		(004)	72.58	29.6	5.81	1.301	5.207	0.057	1.88
ZnO300	300	(002)	34.42	28.3	5.13	2.604	5.209	0.078	2.19
		(004)	72.58	45.7	3.76	1.302	5.208	0.061	3.55

d – thin film thickness, (hkl) – Miller indices corresponding to diffraction planes, θ – Bragg angle, β – half-width of the diffraction peak, D – size of the crystallites [40], d_{hkl} – interplanar spacing, c – crystal lattice constant; with λ = 1.54 Å, wavelength of the incident radiation and $\varepsilon 2$ – tensions along the axis c [39], TC (hkl) – texture coefficient of the (hkl) plane [41,42].

The 300 nm thick ZnO film proved to be improved in structural performance as compared to the other films obtained under similar deposition conditions. This conclusion is supported by the increase in size of the ZnO crystallites and values of the texturing coefficient, which are greater than 1, showing that a larger number of crystallites are oriented with the (hkl) planes parallel to the substrate surface. The narrower the diffraction peaks, the larger the crystallite size. The lattice parameters for the deposited films have lower values than the standard ones [39]. This can be attributed to the fact that the films are made without being subjected to a thermal treatment, which induces an internal stress in the ZnO thin films. To the same extent, the depositions being made at room temperature on all SiO_2 thin films, their structure proved to be essentially amorphous [28,37] with no sharp XRD reflection lines and featuring a matte surface. Based on XPS measurements it was evaluated the effect of increasing the thickness on the deposited samples and oxidation states of each element. The properties of SiO_2 thin films were also determined, noting the preservation of the stoichiometry and purity of the preparation technique.

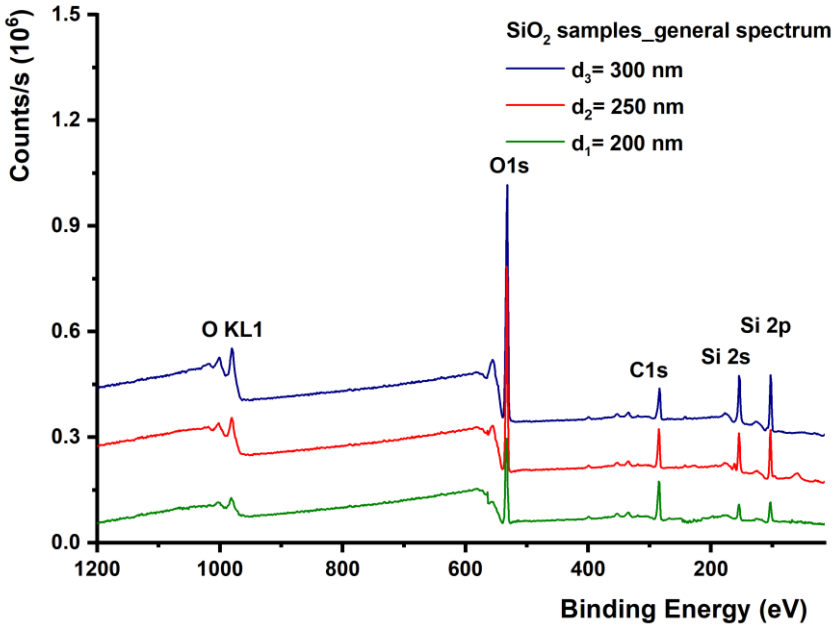

Fig. 2 XPS patterns for SiO_2 thin films: general spectra.

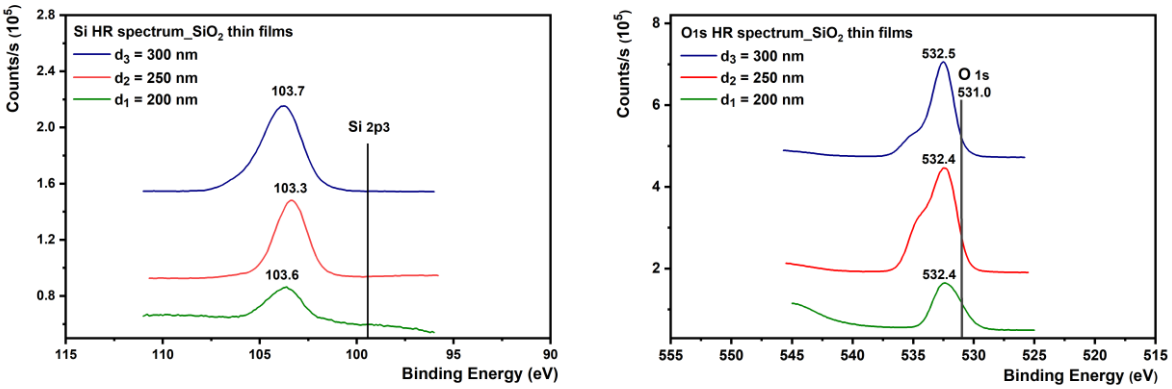

a) b)

Fig. 3 High-resolution XPS spectra acquired from SiO_2 samples: a) Si 2p3 and b) O 1s.

To keep the contamination layer from the surface of the films, they were not sputtered using the ion gun. This is because sometimes the sputtering affects the stoichiometry of the samples by depleting the films of oxygen. Figure 2 shows the general oxide spectra for three SiO_2 samples.

The high resolution (HR) analysis Si 2p3 and O 1s spectra recorded [43,44] for the SiO_2 samples are shown in Figs. 3a and 3b. Using this analysis, we determined the elemental composition as well as the chemical and electronic states of the elements that exist in the SiO_2 films. Although Si 2p3 shows small chemical changes, the binding energy value of 103.7 eV indicates a completely oxidized Si for the SiO_2 films (Fig. 3a). [43-46]. Experimental data reveal that there is good stoichiometry for this film.

The general spectra of ZnO samples are shown in Fig. 4, where peaks corresponding to C 1s, O 1s and Zn 2p were identified for all investigated samples. The presence of photoelectron signals, ZnO electrons and carbon contamination at the binding energy value of 284.8 eV, in the inherently contaminated film are observed.

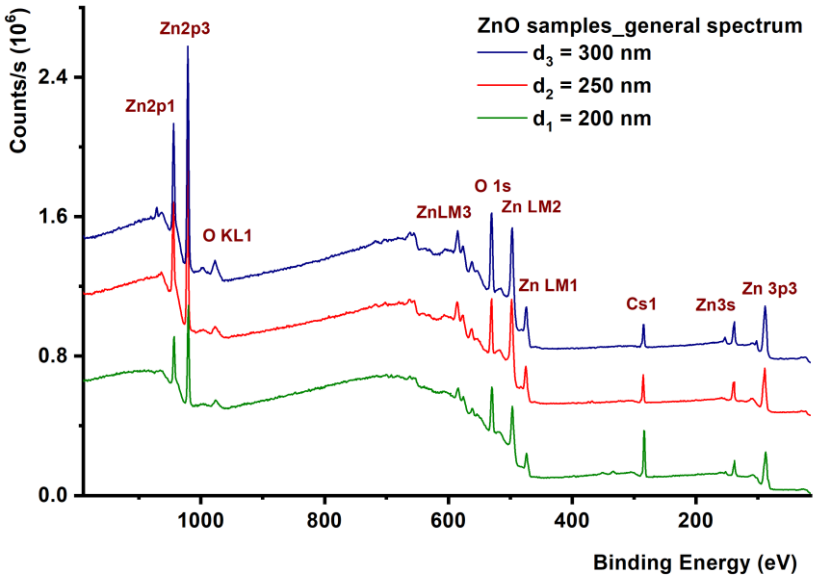

Fig. 4 XPS survey spectra acquired from ZnO films.

This carbon contamination obviously decreases as the film thickness increases; increases in Zn 2p and O 1s intensities are also observed [47,48]. Figures 5 a) and b) show the HR spectra of electron distribution at Zn 2p and O 1s levels, recorded for the ZnO samples.

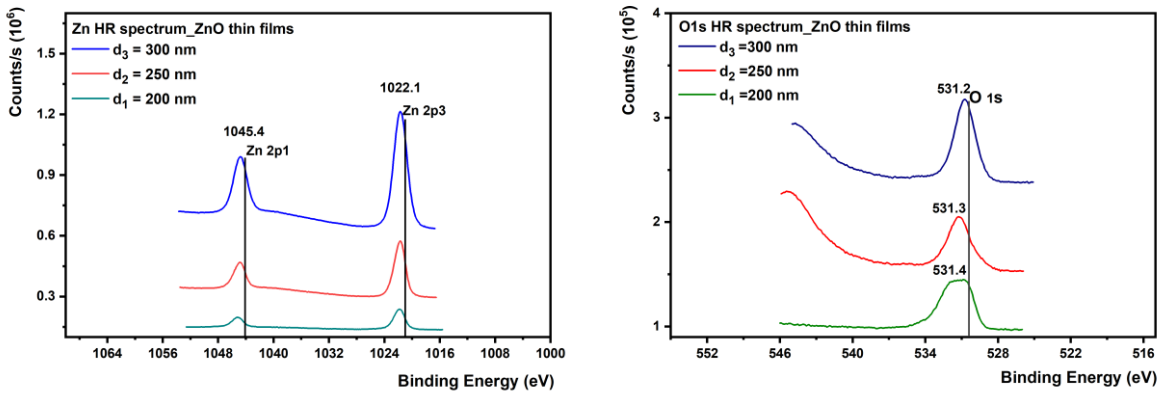

a) b)

Fig. 5 High-resolution a). Zn 2p3 and b). O 1s XPS spectra acquired from ZnO samples.

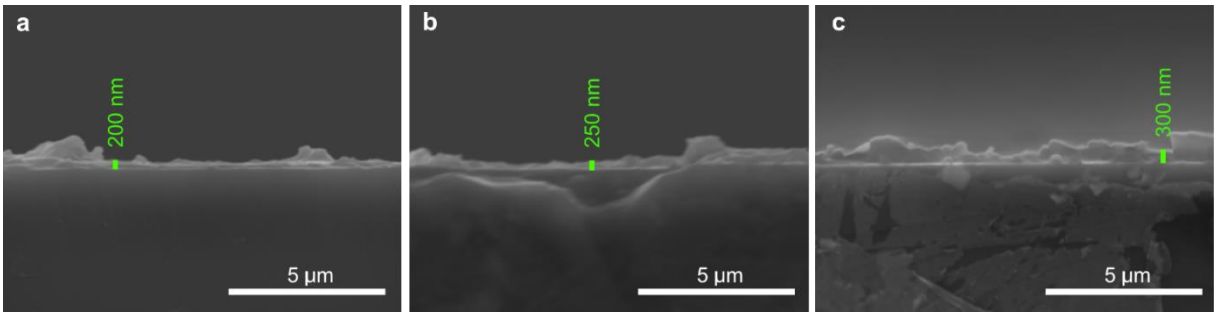

Fig. 6 Cross-sectional SEM images of the cleaved SiO_2 films with measured thickness values of: a) *d*SnO_2_200= 200 nm, b) *d*SnO_2_250 = 250.3 nm; c) *d*SnO_2_300 = 300 nm.

As we can see in Fig. 5a, the Zn 2p spectrum contains a doublet with binding energy (1022.1 eV and 1045.4 eV); they correspond to the Zn 2p3 and Zn 2p1 lines [47]. The presence of metallic zinc is not observed in the general spectrum, which indicates that we have only oxidized zinc in the film. These results are in good agreement with those in the literature [47-49]. Using a magnification of 20.000 ×, the SEM analyzes show small structural changes in the quality of the SiO_2 and ZnO films, proportional with their increase in thickness. SEM cross-section images (Figs. 6a) b) and c)) show films with a dense, homogeneous and uniform surface. For ZnO samples, there is a tendency for self-structuring of the deposited films, as depicted in the SEM images (Figs.7a) b) c)).

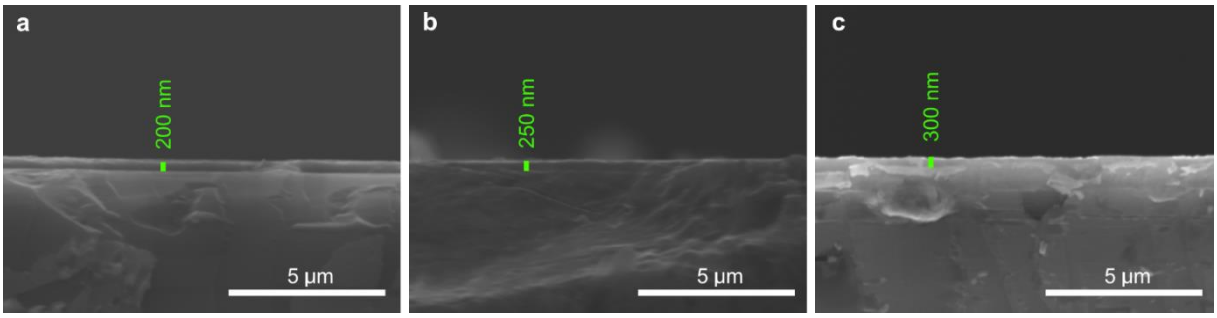

Fig. 7 Cross-sectional SEM images of the cleaved ZnO films with measured thickness values of: a) *d*ZnO200 = 200 nm, b) *d* ZnO250 = 250 nm and c) *d* ZnO300 = 300.2 nm.

The analysis of optical properties, by the absorption of light in the dielectric films of ZnO and SiO_2 with various thicknesses, and determination of the optical constants is useful for their integration in the design and construction of metamaterial structures.

The measured thickness values for oxide films are shown in Table 2, and they are found to be similar with the predefined ones. EDS distribution in all investigated samples caused the appearance of chemical elements like Zn L, Si K and O K (Table 2). It is found that SiO_2 and ZnO films show a better stoichiometry with increasing film thickness (from 200 nm to 300 nm). This is evidenced by the values of atomic concentrations of the analyzed films.

Table 2 Typical chemical composition of SiO_2 and ZnO thin films, determined by EDS measurements.

Sample	***d* (nm)**	**Element**	**Weight %**	**Atomic %**
SiO_2 200	200	O K	35.36	48.38
		Si K	64.64	51.62
SiO_2 250	250	O K	47.11	60.64
		Si K	52.89	39.36
SiO_2 300	300	O K	50.50	65.88
		Si K	49.50	34.11
ZnO 200	200	O K	17.56	45.73
		Zn L	82.44	54.27
ZnO 250	250	O K	18.14	47.52
		Zn L	81.86	52.48
ZnO 300	300	O K	25.85	49.38
		Zn L	74.15	50.62

d – thin film thickness.

In the case of the 200 nm thick SiO_2 sample the percentage composition allowed us to observe the stoichiometry of the sample; respectively, a depletion of oxygen (48.38 %) in the oxide film. For the 250 nm thick SiO_2 sample, and given the percentage data, the finding was that following carbon contamination (according to the XPS investigations) the amount of O K could increase (as compared to the 200 nm thick sample), while the amount of Si K decreases. The atomic concentration of silicon decreases very slightly from 51.62 % to 34.11 %. The EDS analysis of the surface of SiO_2 oxide films illustrates an improvement in the amount of oxygen, as the film thickness increases. In addition, the mass concentration of silicon decreases from 64.64% to 49.50%, accompanied by an increase in the oxide content from 35.36% to 50.50%. For ZnO films, an increase in the film thickness resulted in an increase in the atomic oxide (from 45.73% to 49.38 %), as a result of the plasma-chemical processes.

Optical properties of the films were characterized based on the transmission spectra (Figs. 8 a) and b)), choosing the Swanepoel model to determine the optical constants of the oxide films in the spectral range 190-2500 nm. Wavelength dependence of the transmission coefficient is depicted for the set of SiO_2 and ZnO samples with different thicknesses.

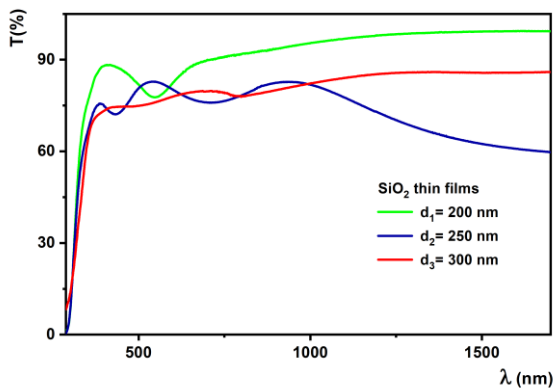

a)

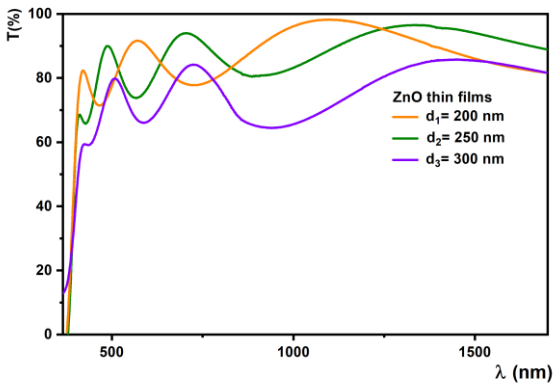

b)

Fig. 8 Transmission spectra of thin films with various thickness values (200nm, 250nm, 300 nm): a) SiO_2 and b) ZnO.

The presence of maxima and minima in the transmission spectra of SiO_2 and ZnO thin films allows for determination of their optical constants, with the help of the envelope method proposed by Swanepoel [50,51]. It was found that thinner samples have a transmission in the range 78 – 92 % while thicker ones in the range 82 – 65 %, for radiation with wavelength of 600 nm. Stronger absorption of the 300 nm thickness thin films is influenced by the increase in the volume of inter-crystalline regions [52].

Optical constants were calculated for both high and low absorption ranges. In the case of transparent SiO_2 and ZnO thin films, between the extinction coefficient, *k*, (Figs. 9 a) and b)) and the absorption coefficient, α, there is the following relation:

$$\alpha = \frac{4\pi k}{\lambda}, \qquad (1)$$

where λ is the wavelength.

We determined the optical bandgap, corresponding to the direct optical transitions, by extrapolating the linear portion of the dependency $(\alpha h\nu)^2 = f(h\nu)$ to $(\alpha h\nu)^2 \rightarrow 0$.

The edge of the absorption band shifts to longer wavelengths with the increasing thickness of the thin films (Figs. 10 a) and b)). In such dielectric materials the electrons are characterized by a high energy bandgap [53].

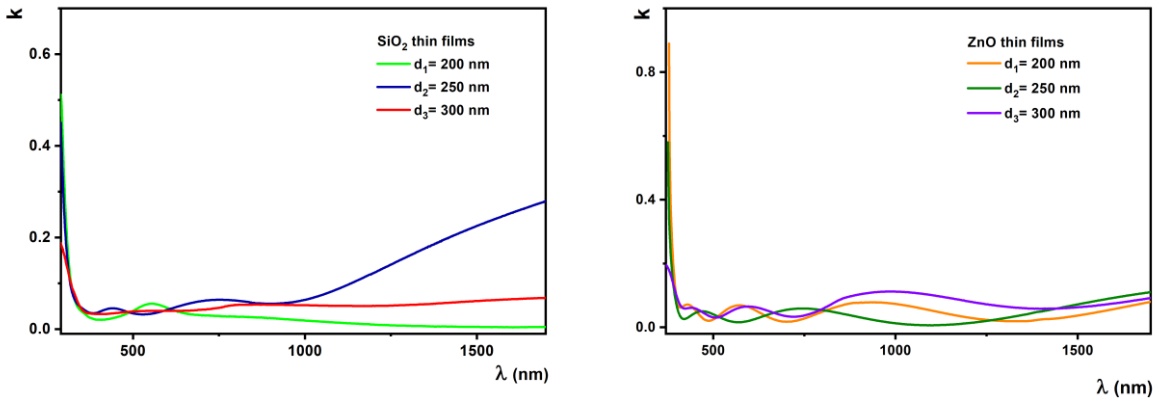

a) b)

Fig. 9 Extinction coefficient dependence on the wavelength for: a) SiO_2 and b) ZnO thin films.

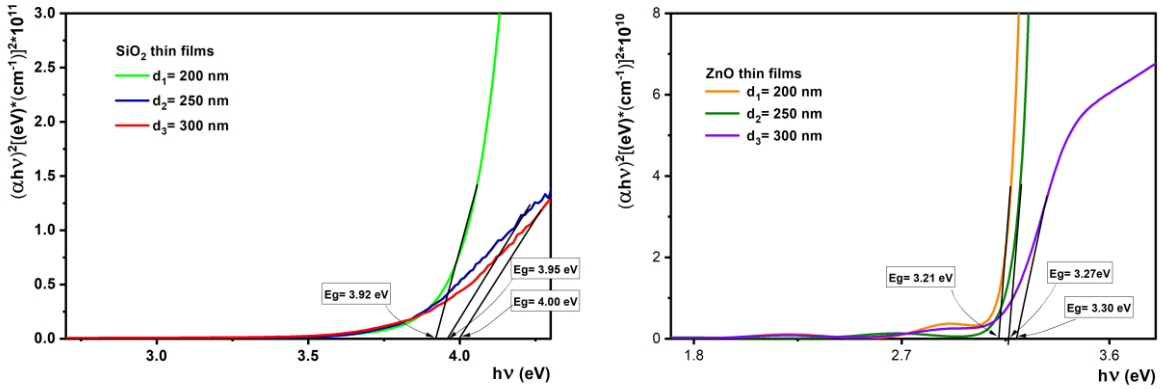

a) b)

Fig. 10 Dependence of $(\alpha h\nu)^2 = f(h\nu)$ on the energy of the incident photons for: a) SiO_2 and b) ZnO samples, with different thickness values.

Bandgap value was determined for all sets of samples, obtaining values between 3.92 – 4.0 eV for SiO_2 samples and 3.2 – 3.3 eV for ZnO films. The band difference of the ZnO films indicated a direct band-to-band transition between the valence and conduction band, while the film stress determined the improvement of the bandgap.

It is found that the bandgap values, corresponding to direct transitions, are similar to those obtained by other researchers [54,55]. These optical properties of ZnO and SiO_2 films have proven to be very important for their use in metamaterial structures. With increasing thickness of the SiO_2 and ZnO films the transmission in the visible range decreases and the porosity at the film surface increases, which is justified by the lack of applied heat treatment.

The dispersion of the refractive index for the investigated samples shows a normal dispersion in the considered spectral range (Figs. 11a) and b)). The plots indicate that

at a wavelength of 430 nm the refractive index of the films approaches minimum value. The quality of dielectric materials is also determined by the dielectric constant values.

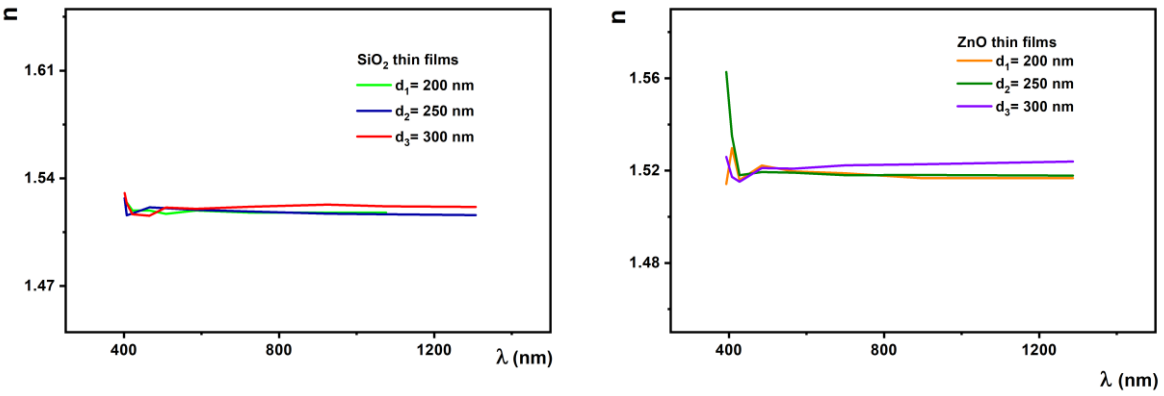

a) b)

Fig. 11 Refractive index dependence on the wavelength (dispersion) for the SiO_2 and ZnO thin films.

Values of the dielectric constant were obtained by using the Drude method [56,57] and spectral absorption of the oxide films. This allowed the assessment of the permittivity and polarizability of the material, as well as the density of states in the band interval. Based on calculus, the value of the real dielectric constant (*εr*) has the formula:

$$\varepsilon r = n_2 - k_2, \quad (2)$$

and the relationship to compute the imaginary dielectric constant is as follows:

$$\varepsilon i = 2nk, \quad (3)$$

where *n* is the refractive index and *k* is the extinction coefficient.

Figures 12 (*i*) and (*ii*) shows the variations of real and imaginary parts of the dielectric constants of ZnO and SiO_2 films with photon energy. It can be seen that the value of the real part is higher than the imaginary one, which is more evident in the 300 nm thick sample. The attractive characteristics of the thickest sample (i.e., 300 nm)

suggest that optimal deposition conditions have been found for real performance, and possibility to be integrated in the metamaterial structures.

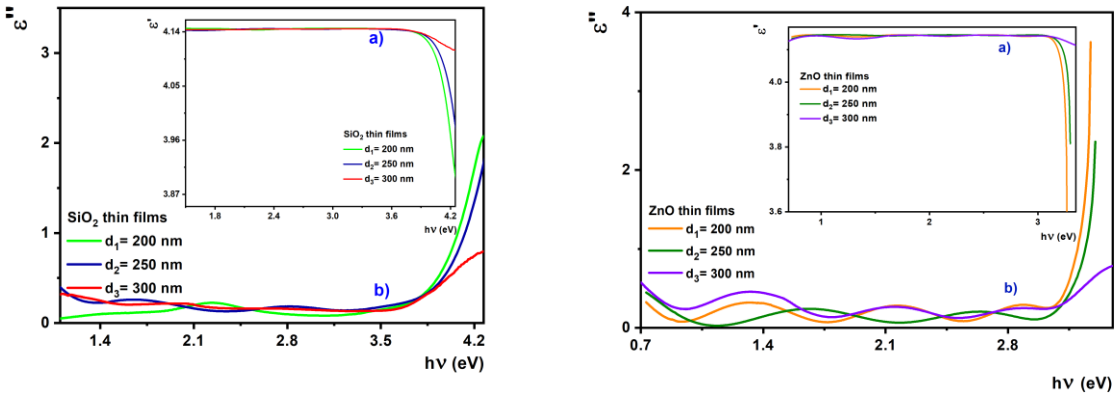

(*i*) (*ii*)

Fig. 12 Photon energy dependence of the: a) real and b) imaginary part of permittivity for the SiO_2 (*i*) and ZnO (*ii*) thin films, with different thickness.

Thus, increasing the thickness of ZnO and SiO_2 films by 100 nm, from 200 nm to 300 nm, improves the quality of samples by 12% – 15%, resulting in a better stoichiometry, increased crystallinity, improved optical and dielectric properties.

Conclusions

SiO_2 and ZnO oxide thin films of various thicknesses were deposited by radio frequency magnetron sputtering technique. Films with a good stoichiometry were obtained as related to the target of provenience. In the case of SiO_2 thin films, they were confirmed by X-ray diffraction measurements that all structures are amorphous. Following X-ray diffraction analyzes, it was proved that the ZnO films show an orientation with the c-axis perpendicular to the substrate surface. The results indicate that the ZnO thin films are crystalline with a hexagonal structure, and with increasing

film thickness the crystallinity of the films as well as the size of the crystallites for the (002) plane increases.

Transmission spectra of the studied oxide films are strongly influenced by the deposition conditions. Smaller values for the transmission coefficient were obtained in the case of thicker samples, such as 74% for ZnO 300 and 68% for SiO_2 300 respectively. The results show that the Swanepoel model describes very well the optical properties of SiO_2 and ZnO films. Also, an improvement of the optical properties of the thin films with increasing thickness was noticed. In conclusion, some of the best quality SiO_2 and ZnO films in terms of structure and optical properties were the 300 nm thick ones. Thus, the attractive characteristics of the thickest sample suggest that optimal deposition conditions have been found, allowing us to obtain samples with real performance to be integrated into metamaterial structures.

Acknowledgements

This research was supported by the ELI [contract number 12/2020] and Program NUCLEU-LAPLAS VI 16N/2019.

References

1. Zeng, X.; Pelenovich, V.; Xing, B.; Rakhimov, R.; Zuo, W.; Tolstogouzov, A.; Liu, C.; Fu, D.; Xiao, X. *Beilstein J. Nanotechnol.* **2020,** *11,* 383-390.

2. Blumenstein, N.J.; Streb, F.; Walheim, S.; Schimmel, T.; Burghard, Z.; Bill, J. *Beilstein J. Nanotechnol.* **2017,** *8,* 296–303.

3. Tkachenko, V.; Marino, A.; Oton, E.; Bennis, N.; Oton, J. M. *Beilstein J. Nanotechnol.* **2016,** 7, 1743-1748.

4. Ashrafi, A.; Jagadish, C. *J Appl. Phys.* **2020,** *127,* 049901.

5. Zhu, X.; Jhang, J.H.; Zhou, C.; Dagdeviren, O. E; Chen, Z.; Schwarz, U. D.; Altman, E. I. *Phys. Chem. Chem. Phys.* **2017,** *19,* 32492-32504.

6. Alver, U.; Tascioglu, M. E.; Guler, O.; Aslan, M.; Yazgan, A.; Kaya, H.; Duran, C.; Cuvalci, H; Bilgin, S. *J. Inorg. Organomet. P.* **2019,** *29,* 1514-1522.

7. Vural, S.; Koytepe, S.; Seckin, T.; Adiguzel, I. *Polym.-Plast. Technol.* **2012,** *51,* 369-376.

8. Chang, L.M.; Hou, Y.; Dong, Z. M. K.; Yan, H. *J. Appl. Phys*. **2007,** *101,* 034101.

9. Paldi, R.L.; Wang, X.; Sun, X.; He, Z.; Qi, Z.; Zhang, X.; Wang, H. *Nano Lett.* **2020,** *20,* 3778-3785.

10. Rogov, A.; Narimanov, E. *ACS Photonics* **2018,** *5,* 2868-2877.

11. Karpov, E. G.; Danso, L.; Klein, J. T. A. *Phys. Rev. E.* **2017,** *96,* 023002.

12. Singh, P.; Thapa, K. B.; Kumar, N.; Singh, D.; Kumar, D. *Results Phys.* **2019,** *1,3* 102346.

13. Tsai, C.Y.; Lai, J.D.; Feng, S.W.; Huang, C.J.; Chen, C.H.; Yang, F.W.; Wang, H.C.; Tu, L.W. *Beilstein J. Nanotechnol.* **2017,** *8,* 1939-1945.

14. Saadaoui, S.; Ben, Y. M. A.; Ben, K.M.; Gharbi, R.; Smecca, E.; Strano, V.; Mirabella, S.; Alberti, A.; Puglisi, R.A. *Beilstein J. Nanotechnol.* **2017,** *8,* 287-295.

15. Das, A. *Curr. Sci. India* **2019**, *117,* 1990-1998.

16.Danewalia, S. S.; Khan, S.; Dhillon, S.; Bansal, N.; Sharma, G.; Singh, K. *Ionics* **2020,** *26,* 2959-2967.

17. Xu, X.; Pruefer, T.; Wolf, D.; Engelmann, H.J.; Bischoff, L.; Huebner, R.; Heinig, K.H.; Moeller, W.; Facsko, S.; von Borany, J. *Beilstein J. Nanotechnol.* **2018,** *9,* 2883-2892.

18. Alipour, A.; Farmani, A.; Mir, A. *Plasmonics* **2020**.

19. Polydorou, E.; Soultati, A.; Vasilopoulou, M. *J. Mater. Chem. C*, **2016***, 4,* 691-703.

20. Marcu, A.; Viespe, C. *Sensor. Actuat. B-Chem.* **2015**, *208,* 1-6.

21. Zhang, H.D.; Liu, Y.J.; Zhang, J.; Zhu, J.W.; Qin, Q.H.; Zhao, C.Z.; Li, X.; Zhang, J.C.; Long, Y.Z. *J. Phys. D Appl. Phys.*, **2018**, *51,* 085102.

22. Jia, C.; Ren, Y.; Yin, Y.; Zhang, W. *Appl. Phys. Lett.* **2019,** *115,* 223503.

23. Schoessler, T.; Schoen, F.; Lemier, C.; Urban, G. *Thin Solid Films* **2020,** *698,* 137877.

24. Socol, M.; Preda, N.; Costas A.; Borca, B.; Popescu-Pelin, G.; Mihailescu, A.; Socol, G; Stanculescu, A. *Nanomaterials-Basel* **2020,** *10,* 468.

25. Radu, A.I.; Filipescu M.; Dumitru, M.; Moldovan, A.; Dinescu, M.; Antohe, S. *Rom. Rep. Phys.* **2020,** *72,* 503.

26.Stoleriu, S.; Lungu, C.; Ghitulica, C. D.; Surdu, A.; Voicu, G.; Cucuruz, A.; Turculet, C. S.; Ciocan, L. T. *Nanomaterials-Basel* **2020,** *10,* 129.

27. Kim, Y. H.; Shin, D. W.; Kim, J. S.; Song, J.H.; Yoon, S.J.; Park, K. B.; Choi, J.W. *Ceram. Int.* **2012**, *38,* S79-S82.

28. Stavarache, I. *Dig. J. Nanomater. Bios.* **2011,** *6,* 1073-1083.

29. Rahmane, S.; Djouadi, M. A. *J. Mater. Sci.-Mater. El.* **2020**.

30. Sultan, M. T.; Maraloiu, A. V.; Stavarache, I.; Gudmundsson, J. T.; Manolescu, A.; Teodorescu, V. S.; Ciurea, M. L.; Svavarsson, H. G. *Beilstein J. Nanotechnol.* **2019,**

31. Rad, Z. S. J.; Afzalzadeh, R. *Sci. Iran.* **2017,** *24,* 3526-3530.

32. Prepelita, P.; Baban, C.; Iacomi, F. *J. Optoelectron. Adv. M.* **2007,** *9,* 2166-2169.

33. Rambu, A. P.; Iftimie N. *B. Mater. Sci.* **2014**, *37,* 441-448.

34. Bai, Y.; Li, Y.; Wang, J.; Fan, W.; Li, Z.; Fu, Y.; Lu, Y. Wang, W. *Integr. Ferroelectr.* **2020,** *207,* 148-155.

35. Schumann, E.; Huebner, R.; Grenzer, J.; Gemming, S.; Krause, M. *Nanomaterials-Basel.* **2018**, *8,* 525.

36. Prepelita, P.; Stefan, N.; Luculescu, C.; Garoi, F.; Birjega, R. *Thin Solid Films* **2012,** *520,* 4689-4693.

37. Stavarache, I.; Ciurea, M. L. *J. Optoelectron. Adv. M.* **2007,** *9,* 2644-2647.

38. Joint Committee on Powder Diffraction Standards *Powder Diffraction File* Card no.36-1451.

39. Flewitt, P.E.Y.; Wild, R.K. *Physical Methods for Materials Characterization*, IOP Publishing LTD, London, 1994

40. Cullity, B.D. *Elements of X-Ray Diffraction*, Addison–Wesley, Reading, MA, 1978.

41. Barret, C.S.; Massalski, T.B. *Structure of Metals*, Pergamon Press, Oxford, 1980.

42. Moholkar, A.V.; Pawar, S.M.; Rajpure, K.Y.; Patil, P.S.; Bhosale, C.H.; *J. Phys. Chem. Solids* **2007,** *68,* 1981–1988.

43. Gorlich, E.; Haber, J.; Stoch, A.; Stoch, J. J. *Solid State Chem*. **1980**, *33, 121*, Element Si, 2p3/2, Formula SiO_2, CAS Registry No. 60676-86-0, Binding Energy 103.7 eV.

44. Miller, M.L.; Linton, R.W.; *Anal. Chem*. **1985**, *57,* 2314, Element O, 1s2, Formula SiO_2, CAS Registry No. 60676-86-0, Binding Energy 532.5 eV.

45. Donley, M.S., Baer, D.R.; Stoebe, T.G.; *Surf. Interface Anal.* **1988**, *11,* 335 Element Si, 2p3/2, Formula SiO_2, CAS Registry No. 60676-86-0, Binding Energy 103.3 eV.

46. Kovacich, J.A.; Lichtman, D; *J. Electron Spectrosc. Relat. Phenom*. **1980**, *18,* 341, Element O, 1s2, Formula SiO_2, CAS Registry No. 60676-86-0, Binding Energy 532.4 eV.

47. Barr, T.L.; Yin, M.; Varma, S.; *J. Vac. Sci. Technol. A* **1992**, *10,* 2383, Element Zn, 2p2/3, Formula ZnO, CAS Registry No. 1314-13-2, Binding Energy 1022.1 eV.

48. Battistoni, C.; Dormann, J.L.; Fiorani, D.; Paparazzo, E.; Viticoli S.; *Solid State Commun.* **1981**, *39,* 581 Element O, 1s2, Formula ZnO, CAS Registry No. 1314-13-2, Binding Energy 531.2 eV.

49. Stavarache, I.; Logofatu, C.; Sultan, M. T.; Manolescu, A.; Svavarsson, H. G.; Teodorescu, V. S.; Ciurea, M. L. *Sci. Rep.-UK.* **2020**, *10 1* 3252.

50.Swanepoel, R. *J. Phys. E: Sci. Instrum*. **1983,** *16,* 1214–1222. doi:10.1088/0022-3735/16/12/023

51. Prepelita, P.; Craciun, V.; Sbarcea, G.; Garoi, F. *Appl. Surf. Sci.* **2014**, *306,* 47-51

52. Bangava, R. (Ed.), *Properties of Wide Bandgap II–VI Semiconductors,* EMIS Inspect, London, 1997.

53. Hodgson, J.N. *Optical Absorbtion and Dispersion in Solids*, Chapman & Hall, London, United Kingdom,1970.

54. Jagadish, C.; Pearson S.J. (Eds.), *Zinc Oxide Bulk, Thin Films and Nanostructures; Processing, Properties and Applications*, Elsevier, Amsterdam, 2006.

55. Alsaad A. M.; Al-Bataineh Q. M.; Ahmad A. A.; Albataineh Z.; Telfah A. *Optik* **2020,** *211,* 164641.

56. Zhao, J.L.; Sun, X.W.; Ryu, H.; Moon, Y.B. *Opt. Mater.* **2011,** *33,* 768–772.

57. Naik, G. V.; Shalaev, V. M.; Boltasseva, A. *Adv. Mater. (Weinheim, Ger.)* **2013,** *25,* 3264–3294.